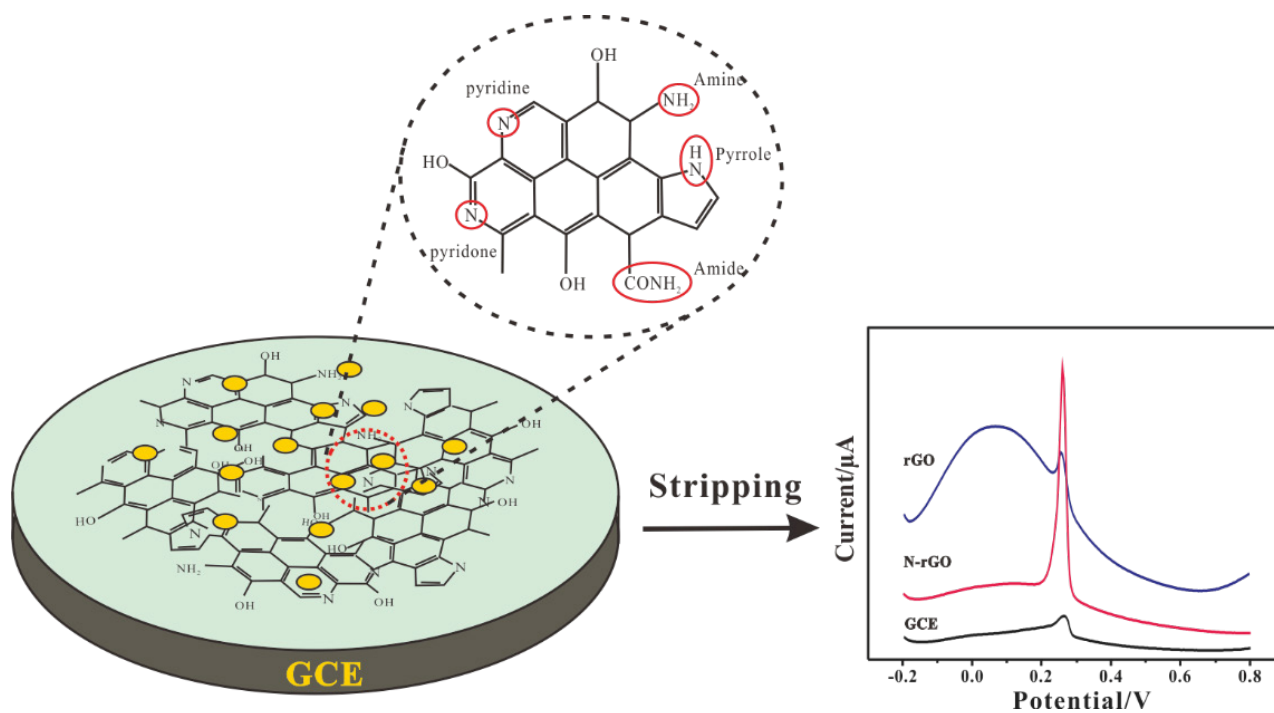


# Fabrication of nitrogen-doped graphene oxide for detection of mercury(II) by electrochemically modified electrodes

Z.G. Wu, C.C. Bi, X. Chen\* and R. Weerasooriya\*



## Highlights

- N-rGO was synthesized by a hydrothermal method with urea used as the N precursor.
- N-rGO modified GCE exhibited an excellent electrochemical response to trace Hg(II).
- The interactions between Hg(II) and N-rGO were computed using Quantum Espresso.
- The Hg(II) detection by N-rGO modified sensor shows minimal interference.

RESEARCH ARTICLE

## Fabrication of nitrogen-doped graphene oxide for detection of mercury(II) by electrochemically modified electrodes

Z.G. Wu<sup>1,2</sup>, C.C. Bi<sup>3</sup>, X. Chen<sup>3,\*</sup> and R. Weerasooriya<sup>1,2,\*</sup>

<sup>1</sup>National Institute of Fundamental Studies, Kandy, Sri Lanka.

<sup>2</sup>Postgraduate Institute of Science, University of Peradeniya, Peradeniya, Sri Lanka.

<sup>3</sup>Institute of Industry and Equipment Technology, Hefei University of Technology, Hefei 230009, PR China.

Received: 30/05/2021; Accepted: 29/10/2021

**Abstract:** Nitrogen-doped reduced graphene oxide (N-rGO) was synthesized by a single-step facile hydrothermal method to modify glassy carbon electrode (GCE) for detection of Hg(II) in water. The electronic properties of graphene and N-rGO were modified using experimental and molecular modelling data. Compared to graphene, N-rGO modified GCE shows enhanced response for detection of Hg(II) with sensitivity of  $19.38 \mu\text{A } \mu\text{M}^{-1}$  and limit of detection (LOD) of 9.29 nM. X-ray photoelectron spectroscopic (XPS) data evidenced the intimate chemical interactions between Hg(II) and N-rGO surface sites. The band structure, bandgap and density of states (DOS) of solid substrates were calculated by density functional theory. The chemical interference of Cd(II), Cu(II), and Pb(II) for detection of Hg(II) by N-rGO modified GCE sensor was minimal. By combining experimental and theoretical data, an efficient method is proposed in materials fabrication required for electrochemical sensors.

**Keywords:** Electrochemical; hydrothermal; Mercury(II) detection; Nitrogen-doped graphene oxide.

### INTRODUCTION

Mercury is a well-known toxicant in human health and the environment (Wang *et al.*, 2004). It is converted into toxic methylated mercury by microorganisms under reducing natural conditions (Abollino *et al.*, 2009; Baird and Cann, 2012; Bridges *et al.*, 2020). Therefore, the development of rapid Hg(II) monitoring methods is a priority. The electrochemical techniques are attractive in detecting Hg(II) species due to their sensitivity, robustness and low-cost (Martín-Yerga *et al.*, 2013). Active substrates for electrochemical sensors are developed using noble metal nanoparticles (Gong *et al.*, 2010b), transition metal oxides (Fayazi *et al.*, 2016) and carbonaceous materials (Wanekaya, 2011) with limited success.

Graphene, a veritable planer carbon material, has many fascinated applications due to its unique materials properties (Fan *et al.*, 2010; Scidà *et al.*, 2018; Li *et al.*, 2019). There are voluminous literature available on the synthesis of graphene nano-composites, such as graphene oxide (GO)/Au (Martín-Yerga *et al.*, 2012; Sahoo *et al.*, 2015), GO/Pt (Pinilla *et al.*, 1996), reduced GO (rGO)/

metal oxide (Fang *et al.*, 2014; Xiong *et al.*, 2015), and DNA-modified rGO (Zhang *et al.*, 2015; Zhang *et al.*, 2016), to modify electrochemical sensors for detection of Hg(II) (Gong *et al.*, 2010a; Chen *et al.*, 2012). However, the complex and costly synthesis procedures associated with nano-composites restrict their applicability.

The electronic properties and edge defects of graphene can also improve by doping it with nonmetallic elements, such as B, S and N (Calandra and Mauri, 2007; Martins *et al.*, 2007; Cervantes-Sodi *et al.*, 2008; Liang *et al.*, 2012). For example, S-doped graphene induces internal modification resulting high propensity of energy density into the substrate (Lee *et al.*, 2015). In a single step, S- and N- synthesized dual-doped graphene showed excellent performance on oxygen reduction compared to Pt/C and S- or N- doped analogues (Liang *et al.*, 2012). The nonmetallic elements doped graphene is also used in fabricating electrochemical sensors for heavy metals detection (Velepini and Pillay, 2019). Use of N-doped rGO/MnO<sub>2</sub> for electrochemical sensing of Hg(II) with enhanced sensitivity has also been reported (Wen *et al.*, 2018). The introduction of active nitrogen groups into the composite remarkably improved the Hg(II) detection capacity, *e.g.*, sensitivity  $124 \mu\text{A } \mu\text{mol L}^{-1}$  and LOD of  $15 \text{ nmol L}^{-1}$ .

Therefore, nitrogen-doped reduced graphene oxide (hereafter N-rGO) was fabricated in this research by a single-step hydrothermal method using urea as an N source to modify electrochemical sensors for detection of Hg(II). The nitrogen doping and partial reduction of graphene oxide occurred concurrently. Modification of glassy carbon electrodes (GCE) was done using N-rGO to develop a highly sensitive and selective Hg(II) detection method. The usage of urea is encouraged due to its abundance, low cost and environmental benignness.

### MATERIALS AND METHODS

#### Materials

Stock solutions of Cd(II), Cu(II), Hg(II) and Pb(II) were prepared using analytical grade cadmium chloride

\*Corresponding Author's Email: [xingchen@hfut.edu.cn](mailto:xingchen@hfut.edu.cn); [rohan.we@nifs.ac.lk](mailto:rohan.we@nifs.ac.lk)



<https://orcid.org/0000-0003-2762-7498>, <https://orcid.org/0000-0002-0509-5307>

(CdCl<sub>2</sub>), copper sulfate (CuSO<sub>4</sub>·5H<sub>2</sub>O), mercuric nitrate [Hg(NO<sub>3</sub>)<sub>2</sub>] and lead nitrate [Pb(NO<sub>3</sub>)<sub>2</sub>], respectively. The following buffers were used to regulate solution pH; 0.10 mol L<sup>-1</sup> CH<sub>3</sub>COONa/CH<sub>3</sub>COOH (ABS), 0.10 mol L<sup>-1</sup> KH<sub>2</sub>PO<sub>4</sub>/0.10 mol L<sup>-1</sup> Na<sub>2</sub>HPO<sub>4</sub> (PBS), and 0.10 mol L<sup>-1</sup> Na<sub>3</sub>C<sub>6</sub>H<sub>5</sub>O<sub>7</sub>/0.10 mol L<sup>-1</sup> C<sub>6</sub>H<sub>8</sub>O<sub>7</sub> (CBS) buffers.

### Synthesis of nitrogen-doped graphene (N-rGO)

Modified Hummers' method was used to synthesize graphene oxide (GO) from flake graphite samples (Hummers and Offeman, 1958). The graphene oxide and urea nano-composite were synthesized by a hydrothermal method. A sample of 40 mg of GO powder were dispersed in 80 mL deionized water and ultra-sonicated for 30 min. Thereafter, a sample of 2 mmol of urea was added to the graphene suspension and stirred till the contents were dissolved. The mixture was then transferred into a Teflon-lined autoclave (100 mL capacity), heated at 180 °C in an electric oven for 12 h and cooled to room temperature. The resulting black product was centrifuged, washed with deionized water several times, and dried at 60 °C for 24 h. The graphene and urea nano-composite are designated as N-rGO.

### Fabrication of chemically modified GCE

The glassy carbon electrode (GCE) was thoroughly polished with 0.1 μm, 0.3 μm and 0.05 μm alumina slurries to a mirror shiny surface.

The cleaned GCE was further sonicated with ethanol and deionized water for 2 min to remove any surface absorbed impurities. An aliquot of N-rGO suspension was pipetted onto the polished GCE surface and dried under nitrogen. GCEs modified with rGO were also prepared using the same method for comparison. The surface sites of the sensor were regenerated by polishing them before the subsequent measurement.

### Materials characterization

The microstructure and morphology of the materials were observed by scanning and transmission electron microscopic methods (SEM, Quanta 200 FEI Company, USA, Acceleration voltage: 5 kV; TEM, JEM-2100, Japan, Electron gun: ZrO/W (100) Schottky, Acceleration voltage: 160 kV). X-ray photoelectron spectroscopy (XPS) analysis was carried out on a VG ESCALAB MKII with Mg Kα (1253.6 eV, 120 W) monochromatic X-ray source. Structural characteristics of the samples were determined using Fourier transform infrared (FTIR) spectrophotometer (Nicolet 67, Thermo Nicolet Co., USA) in the specular transmission mode; the spectra were recorded in the wavenumber range of 500 - 4000 cm<sup>-1</sup>. Further, Raman spectra were obtained with Ar<sup>+</sup> laser excitation at a wavelength of 532 nm (LabRAM HR800 HORIBA Jobin Yvon, FR). The specific surface area of samples was determined using the multipoint BET method (BET, Quantachrome Instruments, USA).

### Electrochemical measurements

All measurements were carried out using a CHI 760E electrochemical analyzer (ChenHua Instruments Co., Shanghai, China) equipped with a three-electrode system: bare or modified GCE working electrode, Pt counter electrode and Ag/AgCl reference electrode (standard electrode potential is +0.2224 V at 298 K). The performance of the modified GCE was determined by cyclic voltammetry (CV). Electrochemical impedance spectroscopy (EIS) was used to determine the electron transfer kinetics of redox systems (Chitravathi *et al.*, 2010; Xu *et al.*, 2013). 5 mmol L<sup>-1</sup> Fe(CN)<sub>6</sub><sup>3-/4-</sup> in 0.10 mol L<sup>-1</sup> KCl solution was used to develop a CV (potential scanning range -0.2 V to 0.6 V and a scan rate of 0.1 V s<sup>-1</sup>). The frequency range used for EIS measurements was 100,000 - 1 Hz. Detection of Hg(II) was carried out using N-rGO modified GCE in 0.1 mol L<sup>-1</sup> ABS (pH 5.0) by SWASV under the deposition potential of -1.0 V for 180 s. The other instrumental parameters, such as stepping potential, frequency and amplitude, were set constant throughout experiments at 4 mV, 25 mV and 15 Hz, respectively.

### Adsorption of Hg(II) on the modified electrode

Adsorption of Hg(II) was accomplished out using 30.0 mg rGO or N-rGO, and 100 μmol L<sup>-1</sup> Hg(II). The solid-solution suspensions of both materials were equilibrated for 12 g. Finally, Hg(II) sorbed rGO and N-rGO were washed with deionized water three times and vacuumed dried for 24 h before XPS analysis.

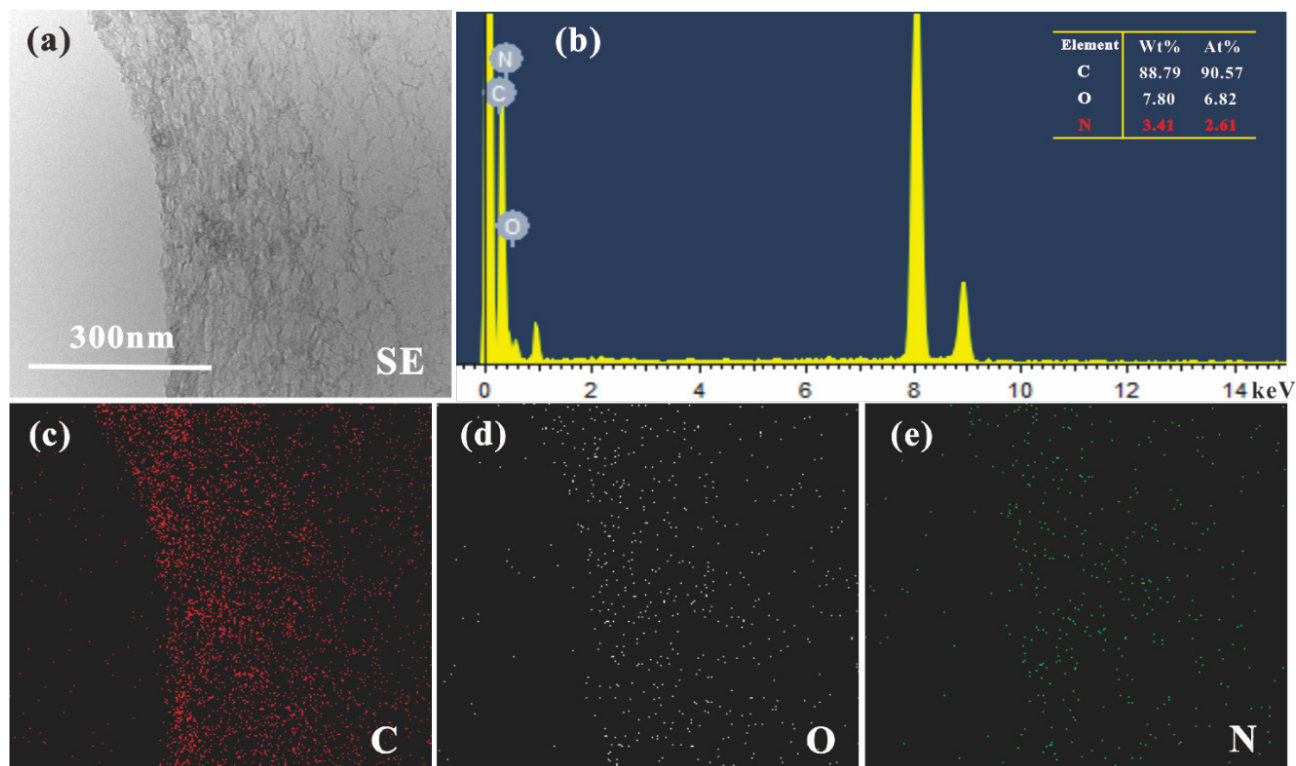
## RESULTS AND DISCUSSION

### Characterizations of N-rGO

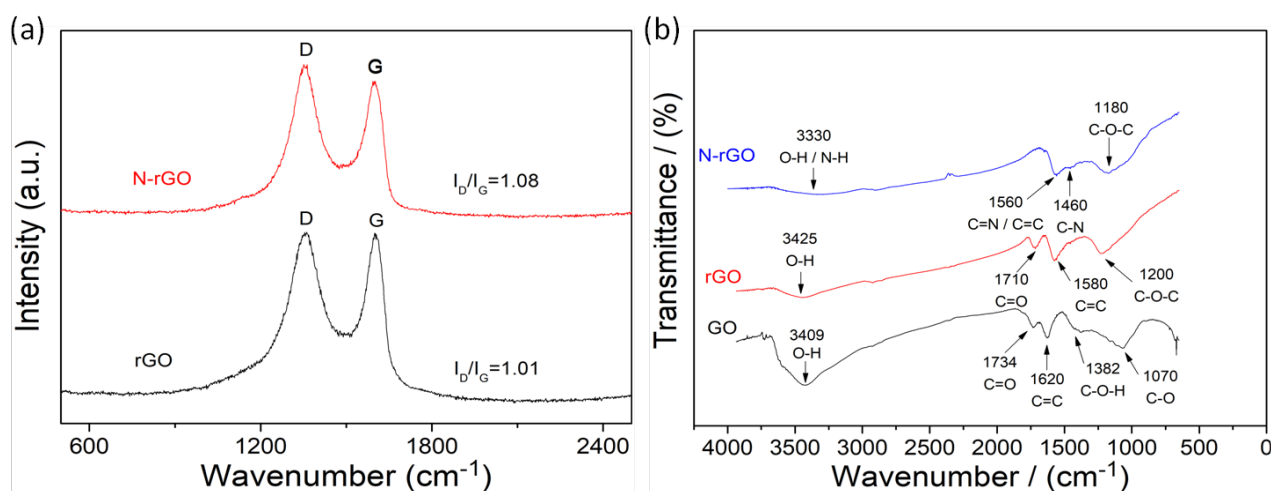
The N-rGO nano-sheets preserve the two-dimensional graphene morphology (Figure 1). The N distribution on the rGO surface is uniform (Figure 1b and 1e). The relative masses of C and N in N-rGO are 88.79% and 3.14%, respectively (EDS data). TEM images together with EDS element distribution maps show efficient N doping into the graphene structure.

Figure 2a shows characteristic D and G Raman bands at 1352 cm<sup>-1</sup> and 1593 cm<sup>-1</sup> for rGO and N-rGO, respectively. The I<sub>D</sub>/I<sub>G</sub> ratio of N-rGO (1.08) is greater than that of rGO (1.01), which indicates topological defects upon N introduction (Suenaga *et al.*, 2000; Lee *et al.*, 2003). The enhanced intensity ratio in N-rGO is ascribed to lattice defects and the sp<sup>2</sup> C stretching vibrations. Consequently, the nitrogen treatment on graphene shows a higher defect density compared to rGO.

Figure 2b shows the FTIR spectra of GO, rGO and N-rGO. The broad bands at 3409 cm<sup>-1</sup> and 1734 cm<sup>-1</sup> are due to solid edge -OH stretching vibrations and C=O deformations (Hontoria-Lucas *et al.*, 1995). The band at 1620 cm<sup>-1</sup> is due to skeletal vibrations of un-oxidized graphite. The bands at 1382 cm<sup>-1</sup> and 1070 cm<sup>-1</sup> are ascribed for C-O-H deformation and C-O stretching vibrations, respectively (Nethravathi and Rajamathi, 2008). The rGO



**Figure 1:** (a) The TEM micrograph and (b) EDS analysis of N-rGO; The related EDS mapping of C (c), O (d), and N (e) in the selected area (a).



**Figure 2:** (a) Raman spectra of rGO and N-rGO, (b) FT-IR spectra of GO, rGO and N-rGO.

retains remnants of O-H ( $3425\text{ cm}^{-1}$ ), C=O ( $1710\text{ cm}^{-1}$ ) and C=C ( $1580\text{ cm}^{-1}$ ) groups showing incomplete GO  $\rightarrow$  rGO reduction. In N-rGO, the band corresponds to the carbonyl group that disappeared after urea reduction. Besides, the wide and strong bands between  $3000\text{ cm}^{-1}$  and  $3700\text{ cm}^{-1}$  contribute to O-H and N-H stretching vibrations in N-rGO (de Graaf *et al.*, 1998). In addition, the band at  $1560\text{ cm}^{-1}$  is due to the  $\text{sp}^2$  C=N and/or C=C (Zhang *et al.*, 1996), and the band at  $1460\text{ cm}^{-1}$  is linked with the  $\text{sp}^3$  C-N (Szörényi *et al.*, 2000). The data confirmed the presence of doped N in graphene.

$\text{N}_2$  adsorption isotherms were carried out to determine the effect of the BET surface area on N doping on rGO (Figure 3a). The BET surface area of rGO is  $31.1\text{ m}^2\text{ g}^{-1}$ ; however, that of N-rGO are increased approximately by

five times ( $145\text{ m}^2\text{ g}^{-1}$ ). The average pore size of N-rGO is smaller than rGO (Figure 3b). The increased surface area and reduced pore size of N-rGO is ascribed to N doping on rGO. The density of active sites on rGO increases upon N doping. The N-rGO shows enhanced sensitivity for the Hg(II) detection.

XPS survey spectra of rGO and N-rGO are shown in Figure 4a. The N 1s peak is distinct for N-rGO. The peaks at 284.08, 399.08 and 531.08 eV correspond to C 1s ( $\text{sp}^2$  C), N 1s and O 1s, respectively. The C 1s N-rGO spectrum is deconvoluted into three components. The peak at 284.77 eV corresponds to the graphite-like  $\text{sp}^2$  C in conjugated honeycomb N-rGO lattice. The small peaks at C2 (285.48 eV) and C3 (287.73 eV) reflect the N- $\text{sp}^2$  and N- $\text{sp}^3$  C-N bonds, respectively, resulting from the N

atoms' substitution for the defects sites on graphene sheets. (Marton *et al.*, 1994; Ronning *et al.*, 1998; Jang *et al.*, 2004). As shown in Fig. 4c, the N 1s peak also splits into three peaks. The peaks at N1 (398.76 eV), N2 (400.00 eV), and N3 (400.91 eV) represent pyridine N, pyrrolic N, and graphitic N atoms, respectively (Wu *et al.*, 1999; Wei *et al.*, 2009). Figure 4d shows the schematic representation of the N-rGO structure. The atomic percentage N in the material is 8.17% (Table 1), higher than rGO, indicating N doped rGO.

### Electrochemical characterization of N-rGO

The cyclic voltammograms and Nyquist plots of GCE, rGO/GCE, and N-rGO/GCE recorded using 5 mmol L<sup>-1</sup> Fe(CN)<sub>6</sub><sup>3-/4-</sup> in 0.1 mol L<sup>-1</sup> KCl are shown in Figure 5. The oxidation and reduction currents resulted from N-rGO modified GCE are determined to be larger than those from rGO (Figure 5a). By introducing N, rGO enhances electron transfer on the electrode surface. A Nyquist plot includes a semicircle and linear portions (Figure 5b). The semicircle at a high-frequency range relates to electron transfer ( $R_{et}$ )

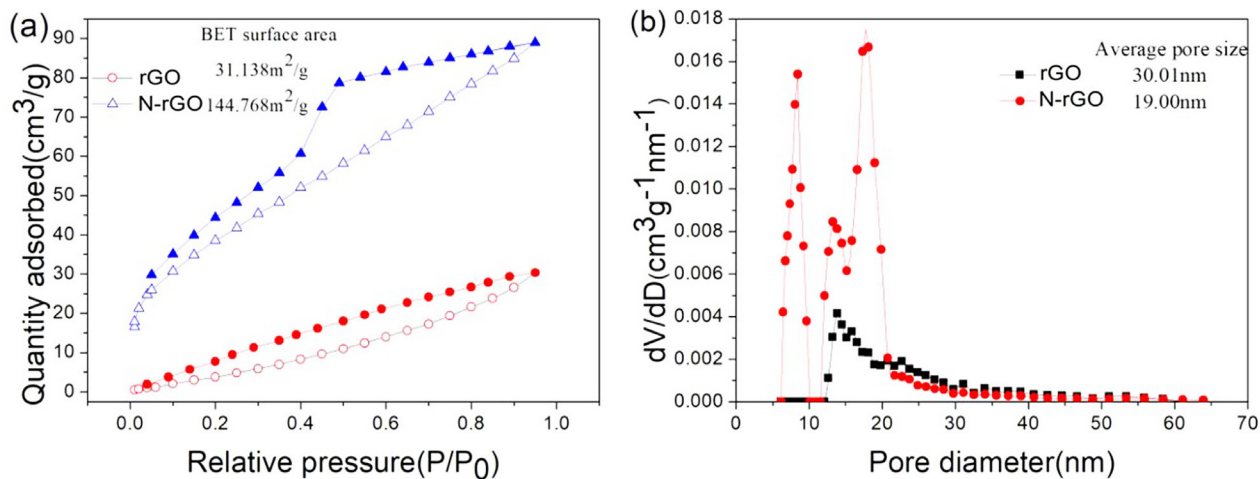


**Figure 3:** (a) Nitrogen adsorption-desorption isotherms and pore size distribution of rGO and N-rGO.

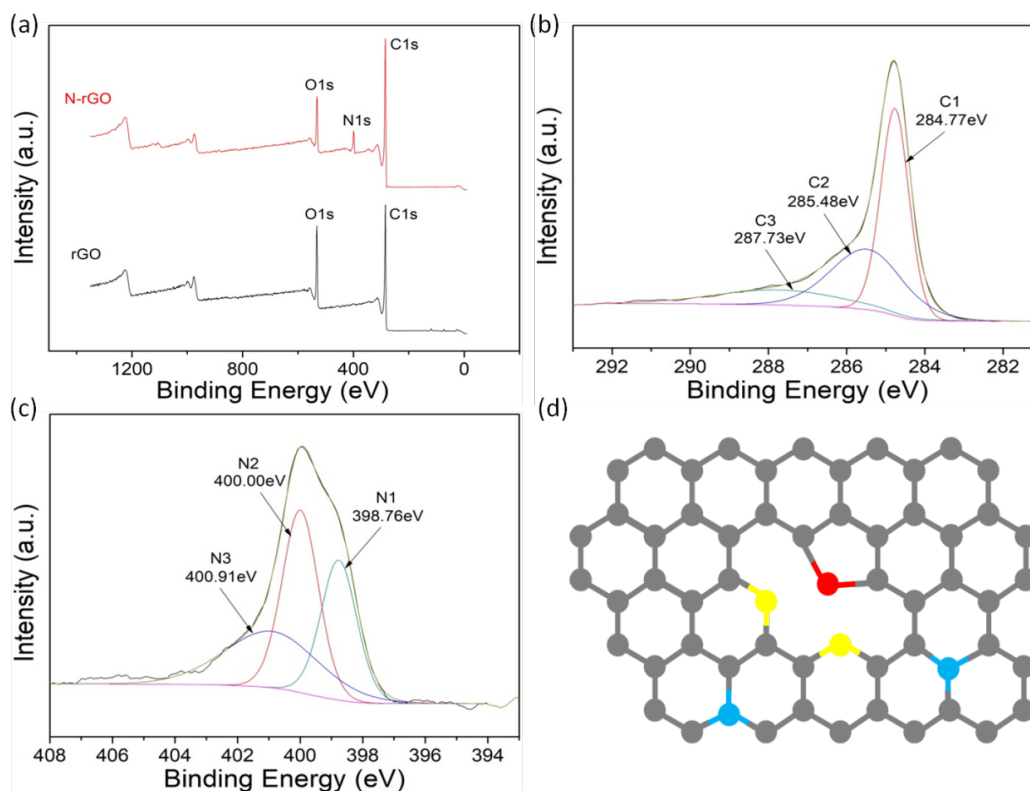


**Figure 4:** (a) The survey XPS spectra of rGO and N-rGO (b) C 1s spectrum (c) N 1s spectrum of N-rGO (d) Schematic representation of N-rGO structure. Gray, blue, yellow and red spheres represent C, graphitic N, pyridine N and pyrrolic N atoms on N-rGO, respectively.

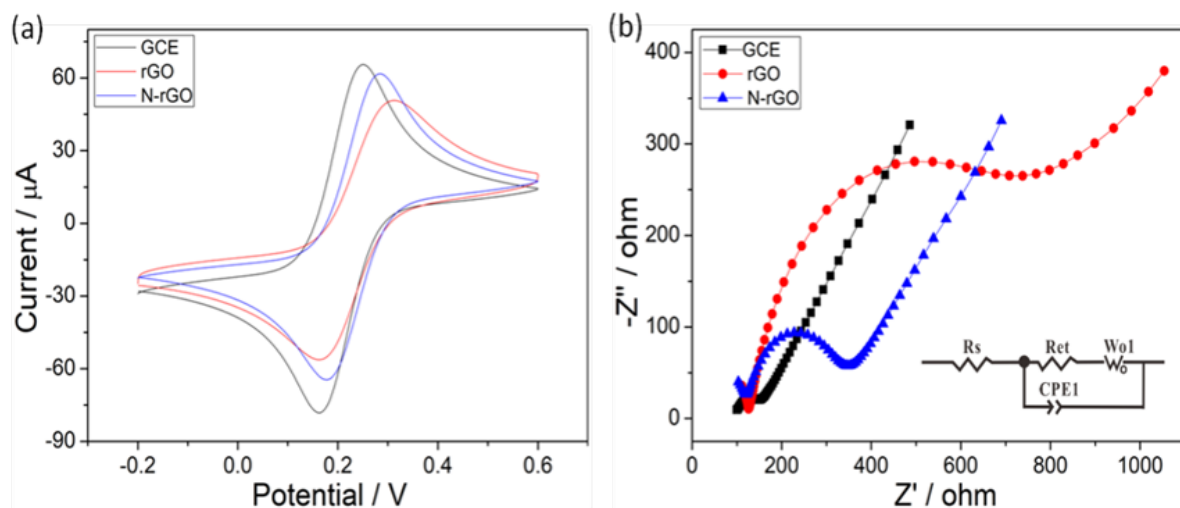


**Figure 5:** CV (a) and EIS (b) were measured with bare GCE, rGO/GCE and N-rGO/GCE in the solution of 5 mmol L<sup>-1</sup> Fe(CN)<sub>6</sub><sup>3-/4-</sup> containing 0.1 mol L<sup>-1</sup> KCl.

**Table 1:** The atomic concentration of C, N and O of hydrothermally synthesized rGO and N-rGO.

Sample	C 1s (%)	N 1s (%)	O 1s (%)
rGO	78.24	0.70	19.99
N-rGO	79.48	8.17	12.35

and solution ( $R_s$ ) resistance controlled by electron transfer dynamics. The linear part of the low-frequency region (45° slope) is consistent with the diffusion-limited process (Han *et al.*, 2016). As shown in Figure 5b, GCE displays a distinct small semicircle domain, implying a low electron transfer resistance of the redox probe. The semicircle domain increases with the rGO modification, indicating that the nano-materials are adhered successfully to the electrode surface. Importantly, the  $R_{et}$  value of N-rGO is lower than that of rGO due to decreased oxygen-containing functional groups on N-rGO.

Further, the circuit simulation analysis on the electrochemical impedance data was also carried out (inset of Figure 5b). The  $R_{et}$  values of GCE, rGO/GCE, and N-rGO/GCE are 156.2  $\Omega$ , 772.3  $\Omega$  and 306.8  $\Omega$ , respectively. Further N-rGO modified GCE shows enhanced electron transfer compared to rGO.

### Electrochemical responses of different electrodes to Hg(II)

To examine the efficiency of different modifiers of GCE electrodes, the bare GCE, rGO/GCE and N-rGO/GCE were selected as sensor materials to determine Hg(II) spike recovery. Figure 6 shows the electrochemical properties of different electrodes to 1.0  $\mu\text{mol L}^{-1}$  Hg(II). The stripping current of N-rGO/GCE is greater than the unmodified GCE, and rGO/GCE shows enhanced N-rGO modified GCE's electrochemical performance.

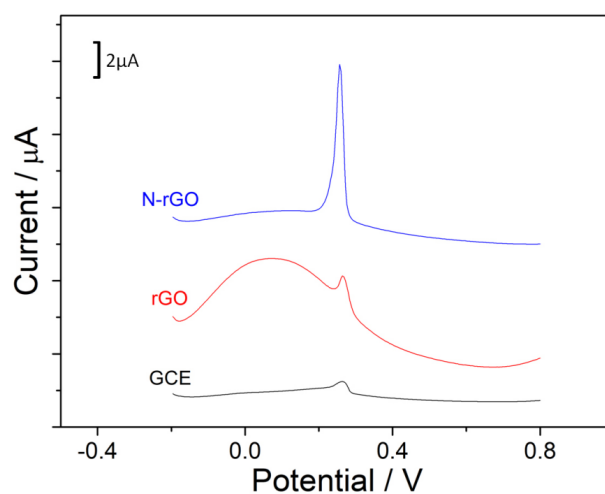


**Figure 6:** Square wave anodic stripping voltammograms for 1.0  $\mu\text{mol L}^{-1}$  Hg(II) on chemically modified GCE in ABS (pH = 5.0). Deposition potential -1.0 V, deposition time 150 s, step potential 4 mV, amplitude 20 mV, frequency 15 Hz.

### Optimal conditions for detection of Hg(II)

The Hg(II) detection efficiency was optimized with respect to type of electrolyte, solution pH, deposition potential and reaction time using 1.0  $\mu\text{mol L}^{-1}$  Hg(II) solution. Figure 7a shows the effects of buffer types for Hg(II) detection. The maximum electrochemical response is observed for ABS compared to PBS or CBS buffers. Accordingly, 0.1 mol L<sup>-1</sup> ABS was used in subsequent experiments.

The intensity of the stripping current peak drops when  $\text{pH} < 4$  or  $> 6$ . At low  $\text{pH} (< 4)$ , the active layer of the electrode surface may deteriorate, decreasing the sensitivity of  $\text{Hg(II)}$  detection; when  $\text{pH} > 6$ ,  $\text{Hg(II)}$  tends to hydrolyze, reducing free  $\text{Hg(II)}$  activity in solution. Therefore,  $\text{pH} 5.0$  was chosen optimally for detection of  $\text{Hg(II)}$ .

Variation of stripping current of  $\text{Hg(II)}$  (range  $-1.1$  to  $-0.6$  V) as a function of deposition potentials was also examined. The overall trend of the stripping current was reduced when the potential varied from  $-1.0$  to  $-0.6$  V due to weak  $\text{Hg(II)}$  adsorption on the electrode surface (Figure 7c). Similarly, the  $\text{Hg(II)}$  response decreases when the potential is less than  $-1.0$  V (Królicka *et al.*, 2006). The hydrogen evolution reaction occurs at negative potentials hindering the electrochemical response of  $\text{Hg(II)}$ .

Figure 7d shows the optimal deposition time for  $\text{Hg(II)}$  detection peak current. As expected, the stripping current has increased with the deposition time. However, the peak current increases gradually up to 150 s, indicating that N-rGO sites are saturated  $\text{Hg(II)}$ . In summary, the optimal conditions for detection of  $\text{Hg(II)}$  by N-rGO modified GCE is as below:  $\text{pH} 5$  ABS,  $-1.0$  V potential and 150 s deposition time at 4 mV step potential, 25 mV amplitude, and 15 Hz frequency. These optimal parameters were used in subsequent measurements.

#### Detection of $\text{Hg(II)}$ by N-rGO modified GCE

The variation of response current as a function of the concentration of  $\text{Hg(II)}$  was measured by N-rGO modified

GCE (Figure 8). The oxidation potential for  $\text{Hg(II)}$  is 0.28 V. The current peak increases linearly within  $0.6$ – $1.6$   $\mu\text{mol L}^{-1}$   $\text{Hg(II)}$ . The linearized equation for detection of  $\text{Hg(II)}$  is  $Y/\mu\text{A} = 19.38 (X/\mu\text{mol L}^{-1}) - 11.03$ , with a sensitivity of  $19.38 \mu\text{A } \mu\text{M}^{-1}$  and limit of detection (LOD) of  $9.29 \text{ nmol L}^{-1}$  based on the  $3\sigma$  method (MacDougall *et al.*, 1980), which is better than the performance of other sensors summarized in Table 2.

#### DFT calculations

The band structure, band gap and density of states (DOS) of graphene, rGO, N-rGO, and  $\text{Hg(II)}$  with N-rGO were computed using Quantum Espresso (QE) (Gumpu *et al.*, 2017; Zhou *et al.*, 2017). The standard density functional theory (DFT) with an optimized kinetic energy cut-off and pseudopotentials were used in the computation. Ultra-soft pseudopotentials described the interactions of the electrons for all the structures (USPP) generated using the PBE method. Gauss smearing technique was used to integrate over the Brillouin zone. The unit cell crystal structures used to compute the band structures of each material is shown in Figure 9.

Graphene has zero-band gap energy showing extraordinary electrical conductivity and electric field effect of  $1013 \text{ cm}^{-3}$  (Wu, 1996; Zhou *et al.*, 2016). The band structure and DOS of graphene exhibit  $0.00 \text{ eV}$  bandgap on the K point in k-paths (Figure 10a). One of the largest issues faced during this computation was selecting k-paths within the Brillouin zone; k-paths were chosen for a hexagonal (HEX, hP) unit cell since the graphene is used as a hexagonal unit cell (Agra-Gutiérrez, Ball and

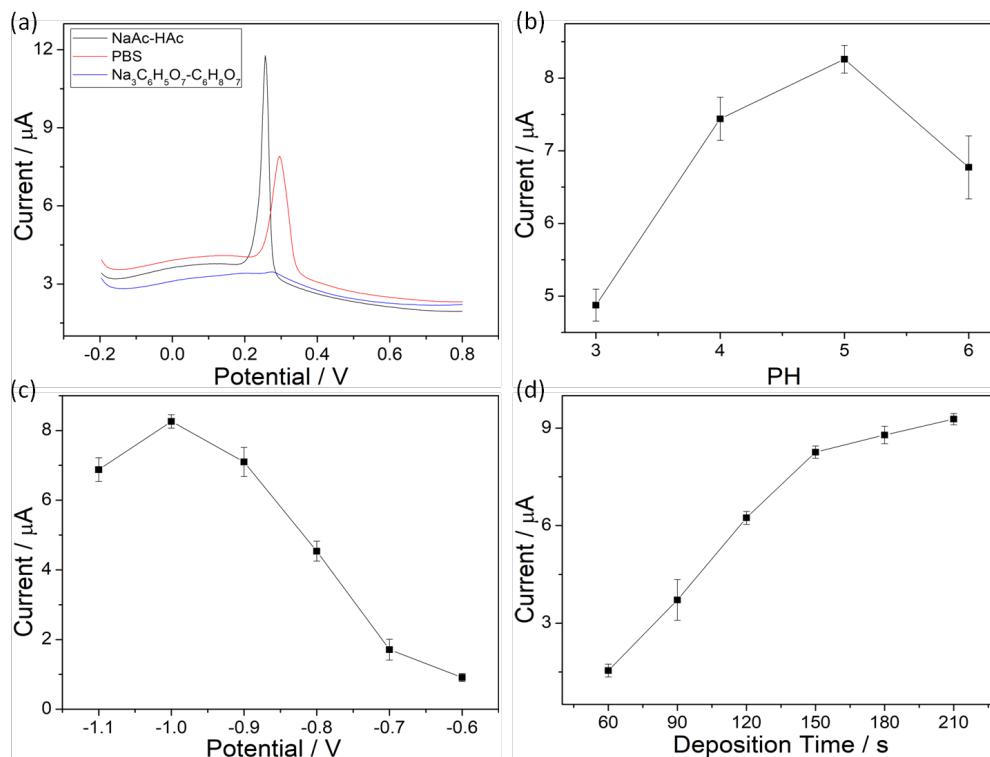


**Figure 7:** The optimum experimental conditions. Influence of (a) supporting electrolytes (b) pH value (c) deposition potential (d) deposition time on the electrochemical responses of the N-rGO nanomaterial modified GCE by SWASV for  $1.0 \mu\text{mol L}^{-1}$   $\text{Hg(II)}$ .

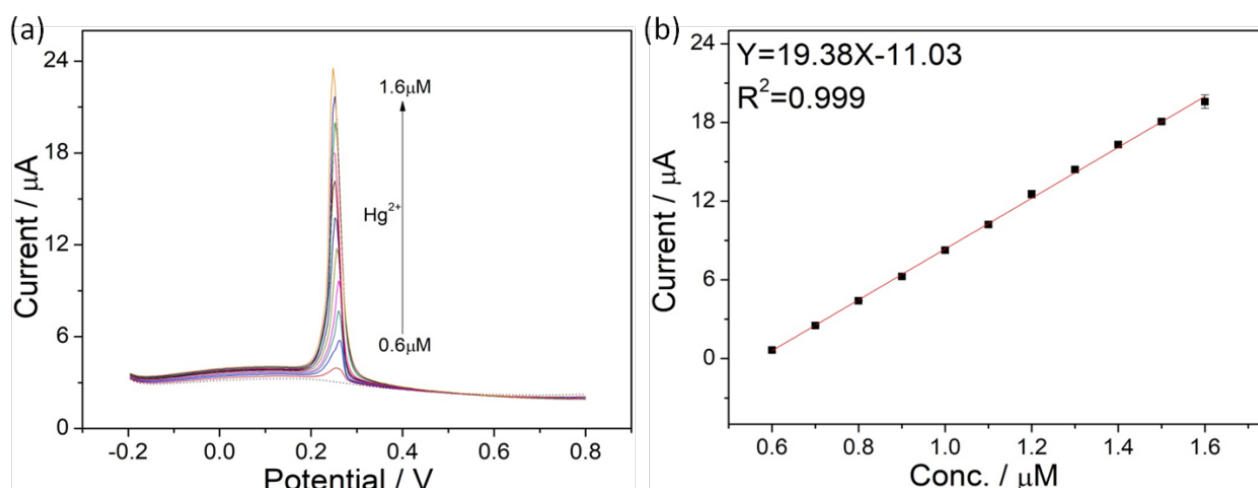


**Figure 8:** SWASV measurements of Hg(II) (a) by N-rGO modified GCE (b) its calibration plot.

**Table 2:** Comparison of current sensitivity and LOD with reported values of different electrodes for electrochemical detection of Hg(II).

Electrodes	Technique in details	Sensitivity ( $\mu\text{A}/\mu\text{mol L}^{-1}$ )	LOD ( $\text{nmol L}^{-1}$ )	Reference
G-MnO <sub>2</sub> /GCE	LSV	0.106	2000	(Lu <i>et al.</i> , 2015)
MnFe <sub>2</sub> O <sub>4</sub> /GCE	SWASV	3.70	-	(Han <i>et al.</i> , 2015)
WBMCPCE NCFs-MCPE	DPASV	4.4833	5	(Rajabi <i>et al.</i> , 2013)
Chitosan-CPE	SWASV	1.27	628	(Marcolino-Junior <i>et al.</i> , 2007)
MnFe <sub>2</sub> O <sub>4</sub> -Cys/GCE	SWASV	11.7	208	(Zhou <i>et al.</i> , 2017)
[Ru(bpy) <sub>3</sub> ] <sup>2+</sup> /GO modified Au	DPASV	3.71	350.20	(Gumpu <i>et al.</i> , 2017)
Fe <sub>3</sub> O <sub>4</sub> -chitosan/GCE	SWASV	9.65	95.7	(Zhou <i>et al.</i> , 2016)
N-rGO/GCE	SWASV	19.38	9.29	This work

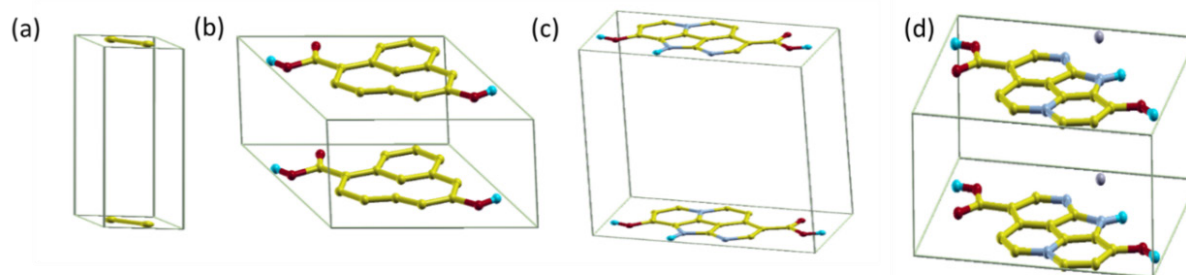


**Figure 9:** Crystal structures are used to compute the band structures of (a) Graphene (b) rGO (c) N-rGO (d) Hg(II) with N-rGO.

Compton, 1998). In contrast, rGO can open up the band gap depending on the amount of oxygen left on the graphene, consisting of sp<sup>2</sup> graphitic islands and oxidized graphene separately (Florence, 1970). According to Figure 10b, the calculated band structures and DOS showed the bandgap of rGO is 0.77 eV. The result obtained indicates the band gap opening for graphene with a reduction of oxygen content. The nitrogen doping into rGO has resulted in three types of bindings: quaternary N (or graphitic N), pyridinic N, and pyrrolic N. All contributed to the  $\pi$  electrons system by modifying electronic properties of N-rGO (Ouyang *et al.*, 2011; Zhou *et al.*, 2016). The estimated N-rGO bandgap is

0.22 eV at the K point. The N atoms and other topological defects act as scattering centres in rGO lattice; the electrical conductivity of N-rGO lowered to 0.55 eV (compared to rGO). Therefore, it confirms that nitrogen doping effectively modifies the electronic structure of graphene lattice (Zhou *et al.*, 2016). To investigate the interaction between Hg(II) and N-rGO, the band structure and DOS of Hg(II) with N-rGO was computed (Figure 10d). The calculated band gap value is 0.27 eV for N-rGO. The introduction of Hg(II) to N-rGO may show less effect on the band gap value. However, increasing the metal ions to N-rGO can efficiently modify the electrical conductivity of

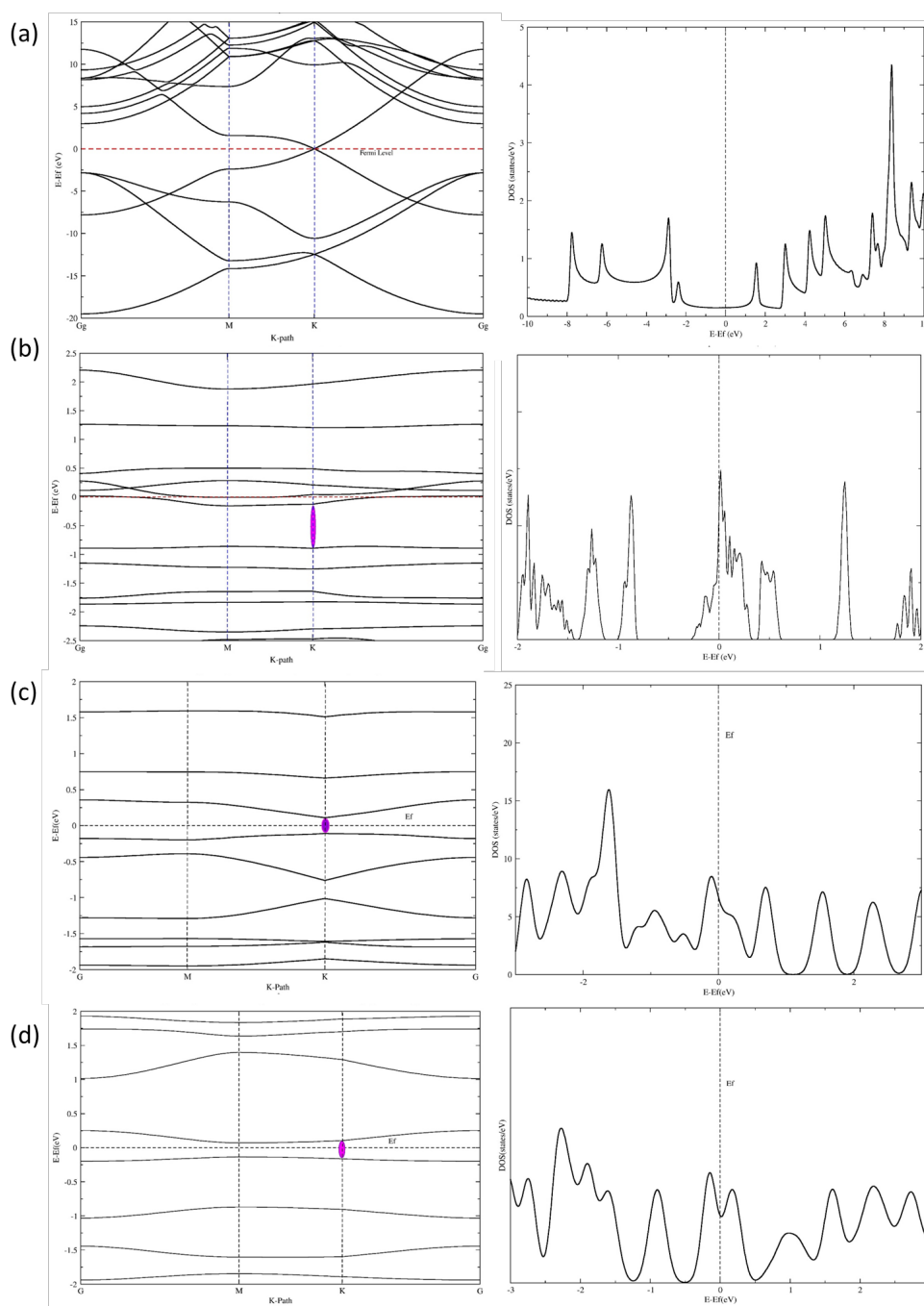


**Figure 10:** Electronic band structure (left) and their corresponding total density of states (right) of (a) Graphene (b) rGO (c) N-rGO (d) Hg(II) with N-rGO, calculated by USPP generated using PBE method.

the material.

### Adsorption of Hg(II) on N-rGO

Adsorption Hg(II) on rGO and N-rGO surfaces was characterized by XPS to determine interactions between N-rGO and Hg(II). The characteristic band of Hg 4f observed in Figure 11a shows the presence of Hg(II) on N-rGO (red spectrum). The relative affinity of Hg(II) adsorption on rGO and N-rGO was also examined (Figure 11b). The intensity of the Hg 4f<sub>1/2</sub> peak in N-rGO is higher than rGO, which implies a strong affinity of Hg(II) on N-rGO sites. On the other hand, the Hg 4f of rGO and N-rGO at 101.20 and 105.20 eV, and 101.15 and 105.30 eV, respectively, are evident. The Hg4f peaks of pure Hg(NO<sub>3</sub>)<sub>2</sub>

are observed at 101.30 eV and 105.40 eV, and a negative shift (0.05 eV) of Hg 4f in N-rGO is observed in comparison with rGO, which implied the strong interaction of N-rGO with Hg(II). In addition, the Hg(II) content in N-rGO was 1.72% compared to a small content of 1.04% in rGO upon adsorption.

### Chemical Interferences for Detection of Hg(II)

In the presence of foreign metal ions, the chemical interferences by Cd(II), Cu(II) and Pb(II) and on the detection of Hg(II) using N-rGO modified GCE was examined. The peak currents of Cd(II), Cu(II) and Pb(II) increased with the addition of Hg(II) due to film formation. Mercury film or mercury-based electrodes are widely used

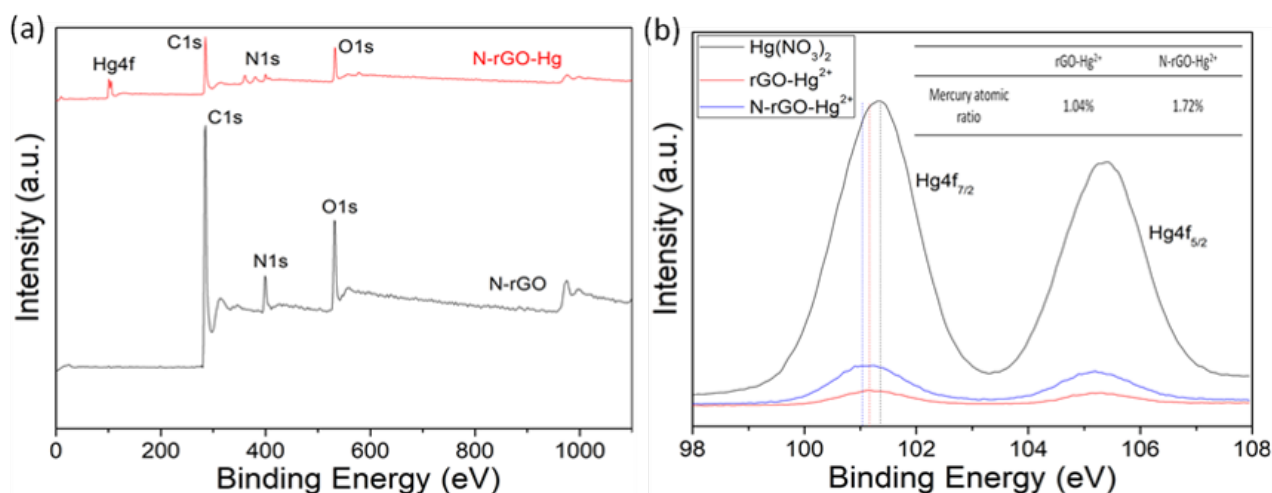


**Figure 11:** (a) X-ray photoelectron spectroscopy survey of N-rGO before adsorption and after adsorption (b) The comparison of N-rGO and rGO in the adsorption of Hg(II). The inset is the mercury atomic ratio of rGO-Hg(II) and N-rGO-Hg(II).

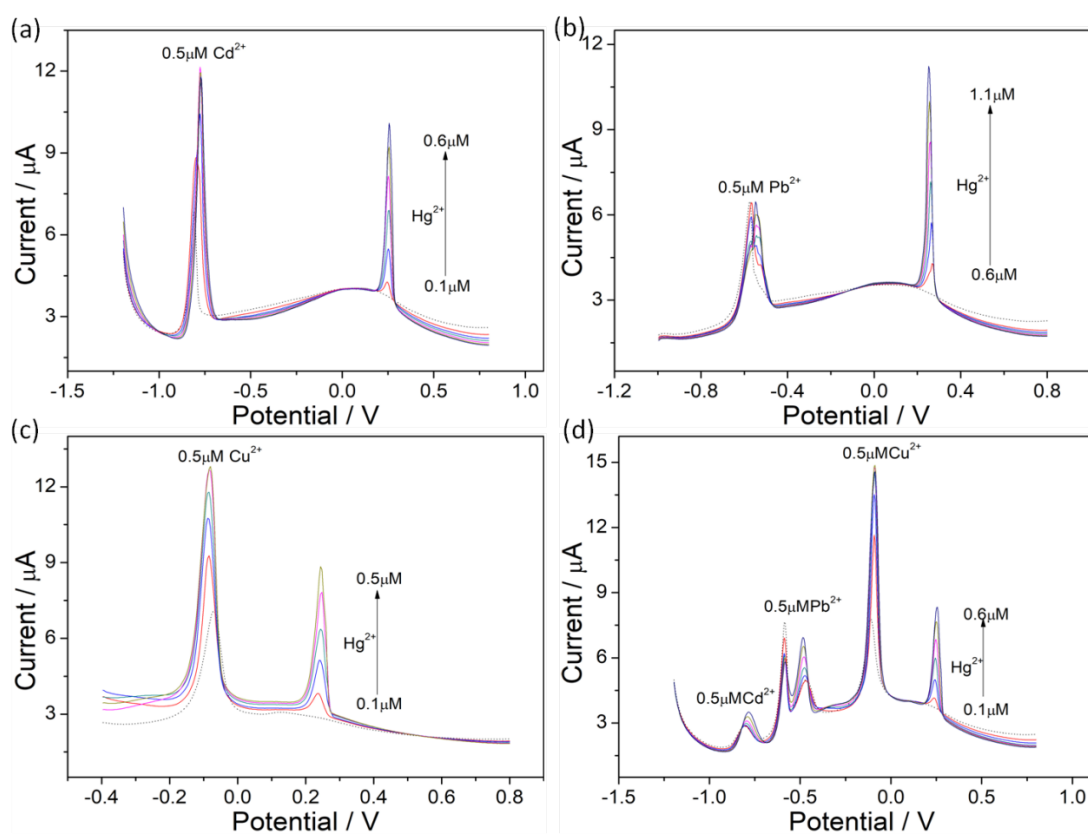


**Figure 12:** SWASV responses of the N-rGO modified GCE for Hg(II) in the presence of other cations (a)  $0.5 \mu\text{mol L}^{-1}$  Cd(II) (b)  $0.5 \mu\text{mol L}^{-1}$  Pb(II) (c)  $0.5 \mu\text{mol L}^{-1}$  Cu(II) (d)  $0.5 \mu\text{mol L}^{-1}$  Cd(II), Pb(II) and Cu(II).

in electrochemical metal ions analysis (Florence, 1970; Wu, 1996; Agra-Gutiérrez *et al.*, 1998; Ouyang *et al.*, 2011). Unfortunately, these electrodes have limited use due to the toxicity of the waste generated.

In the presence of foreign cations, the sensitivity of Hg(II) detection by the N-rGO modified GCE has decreased slightly due to amalgamation and competition for active surface sites. However, the shape of Hg(II) peak

and the correlation coefficient of Hg(II) remain excellent regardless of the interfering cations.

#### Spiked water sample analysis

Detection of Hg(II) was also performed by N-rGO modified GCE using a water sample collected from Hubing Pond (location: Hefei University of Technology (Hefei City, Anhui Province, China). The sample was acidified to pH 5.0 with ABS before measurements. Detection of

**Table 3:** Determination of Hg(II) in real water samples using the proposed method ( $n = 3$ ).

Sample	Added ( $\mu\text{mol L}^{-1}$ )	Found ( $\mu\text{mol L}^{-1}$ )	Recovery (%)
Hubing Pond	0.60	$0.59 \pm 0.007$	$98.3 \pm 1.17$

Hg(II) in the sample was carried out by SWASV using the standard addition method. No Hg(II) was found in the pond water. As shown in Table 3, the spike recovery and relative method error was 98.3% and 1.17%, respectively. The results indicate the applicability of the N-rGO modified GCE for detection of Hg(II) in natural water.

## CONCLUSION

Nitrogen-doped graphene (N-rGO) has been successfully synthesized by a single-step hydrothermal method using graphene oxide and urea as starting materials to fabricate an electrochemical sensor to detect Hg(II) in solution. The N-rGO shows excellent sensitivity ( $19.38 \mu\text{A } \mu\text{mol L}^{-1}$ ) and LOD ( $9.29 \text{ nmol L}^{-1}$ ) to detection of Hg(II) compared with rGO. The nitrogen derived functional groups present in N-rGO play an important role in re-oxidizing metals. The experimental and molecular modelling data confirmed the chemical interactions between Hg(II) and N-rGO. The N-rGO modified GCE has been successfully used for Hg(II) spike recovery experiments in a lake water matrix. Nitrogen doping is efficient in tuning the electronic structure of the graphene lattice. The experimental data associated with theoretical calculations show a promise in fabricating chemically modified electrochemical sensors for rapid monitoring of metal ions.

## ACKNOWLEDGMENT

National Research Council of Sri Lanka is acknowledged for support under the Target Driven Grant Scheme (NRC-TO-16-015).

## DECLARATION OF CONFLICT OF INTEREST

The authors declare no competing financial interest.

## REFERENCES

Abollino, O., Giacomino, A., Malandrino, M., Marro, S. and Mentasti, E. (2009). Voltammetric determination of methylmercury and inorganic mercury with an home made gold nanoparticle electrode. *Journal of Applied Electrochemistry* **39**: 2209 - 2216. DOI: <https://doi.org/10.1007/s10800-009-9830-5>.

Agra-Gutiérrez, C., Ball, J.C. and Compton, R.G. (1998). Anodic stripping voltammetry at a hydrodynamic mercury electrode under high mass transport conditions. 2. experimental verification of theory and implications for sonovoltammetry. *The Journal of Physical Chemistry B* **102**: 7028 - 7032. DOI: <https://doi.org/10.1021/jp982247c>.

Baird, C. and Cann, M. (2012). *Environmental Chemistry*. New York, NY : W.H. Freeman and Company, 5<sup>th</sup> Edition.

Bridges, K.N., Furin, C.G. and Gerlach, R.F. (2020). Subsistence fish consumption in rural Alaska: using regional monitoring data to evaluate risk and bioavailability of dietary methylmercury. *Science of the Total Environment* **736**: 139676. DOI: <https://doi.org/10.1016/j.scitotenv.2020.139676>.

Calandra, M. and Mauri, F. (2007). Electronic structure of heavily doped graphene: the role of foreign atom states. *Physical Review B* **76**: 161406. DOI: <https://doi.org/10.1103/PhysRevB.76.199901>.

Cervantes-Sodi, F., Csányi, G., Piscanec, S. and Ferrari, A.C. (2008). Edge-functionalized and substitutionally doped graphene nanoribbons: electronic and spin properties. *Physical Review B* **77**: 165427. DOI: <https://doi.org/10.1103/PhysRevB.77.165427>.

Chen, K., Lu, G., Chang, J., Mao, S., Yu, K., Cui, S. and Chen, J. (2012). Hg(II) ion detection using thermally reduced graphene oxide decorated with functionalized gold nanoparticles. *Analytical Chemistry* **84**: 4057-4062. DOI: <https://doi.org/10.1021/ac3000336>.

Chitravathi, S., Kumara Swamy, B.E., Chandra, U., Mamatha, G.P. and Sherigara, B.S. (2010). Electrocatalytic oxidation of sodium levothyroxine with phenyl hydrazine as a mediator at carbon paste electrode: a cyclic voltammetric study. *Journal of Electroanalytical Chemistry* **645**: 10 - 15.

de Graaf, A., Dinescu, G., Longueville, J.L., van de Sanden, M.C.M., Schram, D.C., Dekempeneer, E.H.A. and van Ijzendoorn, L.J. (1998). Amorphous hydrogenated carbon nitride films deposited via an expanding thermal plasma at high growth rates. *Thin Solid Films* **333**: 29 - 34. DOI: [https://doi.org/10.1016/S0040-6090\(98\)00762-7](https://doi.org/10.1016/S0040-6090(98)00762-7).

Fan, Z., Yan, J., Zhi, L., Zhang, Q., Wei, T., Feng, J., Zhang, M., Qian, W. and Wei, F. (2010). A three-dimensional carbon nanotube/graphene sandwich and its application as electrode in supercapacitors. *Advanced Materials* **22**: 3723-3728. DOI: <https://doi.org/10.1002/adma.201001029>.

Fang, S., Dong, X., Zhang, Y., Kang, M., Liu, S., Yan, F., He, L., Feng, X., Wang, P. and Zhang, Z. (2014). One-step synthesis of porous cuprous oxide microspheres on reduced graphene oxide for selective detection of mercury ions. *New Journal of Chemistry* **38**: 5935 - 5942.

Fayazi, M., Taher, M.A., Afzali, D. and Mostafavi, A. (2016). Fe<sub>3</sub>O<sub>4</sub> and MnO<sub>2</sub> assembled on halloysite nanotubes: a highly efficient solid-phase extractant for electrochemical detection of mercury(II) ions. *Sensors and Actuators B: Chemical* **228**: 1 - 9. DOI: <https://doi.org/10.1016/j.snb.2016.12.107>.

Florence, T.M. (1970). Anodic stripping voltammetry with a glassy carbon electrode mercury-plated in situ.

- Journal of Electroanalytical Chemistry and Interfacial Electrochemistry* **27**: 273 - 281. DOI: [https://doi.org/10.1016/S0022-0728\(70\)80189-9](https://doi.org/10.1016/S0022-0728(70)80189-9).
- Gong, J., Zhou, T., Song, D. and Zhang, L. (2010a). Monodispersed Au nanoparticles decorated graphene as an enhanced sensing platform for ultrasensitive stripping voltammetric detection of mercury(II). *Sensors and Actuators B: Chemical* **150**: 491 - 497. DOI: <https://doi.org/10.1016/j.snb.2010.09.014>.
- Gong, J., Zhou, T., Song, D., Zhang, L. and Hu, X. (2010b). Stripping voltammetric detection of mercury(II) based on a Bimetallic Au - Pt inorganic - organic hybrid nanocomposite modified glassy carbon electrode. *Analytical Chemistry* **82**: 567 - 573. DOI: <https://doi.org/10.1021/ac901846a>.
- Gumpu, M.B., Veerapandian, M., Krishnan, U.M. and Rayappan, J.B.B. (2017). Simultaneous electrochemical detection of Cd(II), Pb(II), As(III), and Hg(II) ions using ruthenium(II)-textured graphene oxide nanocomposite. *Talanta* **162**: 574 - 582. DOI: <https://doi.org/10.1016/j.talanta.2016.10.076>.
- Han, X.J., Zhou, S.F., Fan, H.L., Zhang, Q.X. and Liu, Y.Q. (2015). Mesoporous MnFe<sub>2</sub>O<sub>4</sub> nanocrystal clusters for electrochemistry detection of lead by stripping voltammetry. *Journal of Electroanalytical Chemistry* **755**: 203-209. DOI: <https://doi.org/10.1016/j.jelechem.2015.07.054>.
- Han, Y., Wang, J., Zhang, H., Zhao, S., Ma, Q. and Wang, Z. (2016). Electrochemical impedance spectroscopy (EIS): an efficiency method to monitor resin curing processes. *Sensors and Actuators A: Physical* **250**: 78 - 86. DOI: <https://doi.org/10.1016/j.sna.2016.08.028>.
- Hontoria-Lucas, C., López-Peinado, A.J., López-González, J.D.D., Rojas-Cervantes, M.L. and Martín-Aranda, R.M. (1995). Study of oxygen-containing groups in a series of graphite oxides: Physical and chemical characterization. *Carbon* **33**: 1585 - 1592. DOI: [https://doi.org/10.1016/0008-6223\(95\)00120-3](https://doi.org/10.1016/0008-6223(95)00120-3).
- Hummers, W.S. and Offeman, R.E. (1958). Preparation of graphitic oxide. *Journal of the American Chemical Society* **80**: 1339 - 1339. DOI: <https://doi.org/10.1021/ja01539a017>.
- Jang, J.W., Lee, C.E., Lyu, S.C., Lee, T.J. and Lee, C.J. (2004). Structural study of nitrogen-doping effects in bamboo-shaped multiwalled carbon nanotubes. *Applied Physics Letters* **84**: 2877-2879. DOI: <https://doi.org/10.1063/1.1697624>.
- Królicka, A., Bobrowski, A. and Kowal, A. (2006). Effects of electroplating variables on the voltammetric properties of bismuth deposits plated potentiostatically. *Electroanalysis* **18**: 1649-1657. DOI: <https://doi.org/10.1002/elan.200603576>.
- Lee, W.S.V., Leng, M., Li, M., Huang, X.L. and Xue, J.M. (2015). Sulphur-functionalized graphene towards high performance supercapacitor. *Nano Energy* **12**: 250 - 257. DOI: <https://doi.org/10.1016/j.nanoen.2014.12.030>.
- Lee, Y.T., Kim, N.S., Bae, S.Y., Park, J., Yu, S.C., Ryu, H. and Lee, H.J. (2003). Growth of vertically aligned nitrogen-doped carbon nanotubes: control of the nitrogen content over the temperature range 900 - 1100 °C. *The Journal of Physical Chemistry B* **107**: 12958 - 12963. DOI: <https://doi.org/10.1021/jp0274536>.
- Li, G., Huang, B., Pan, Z., Su, X., Shao, Z. and An, L. (2019). Advances in three-dimensional graphene-based materials: configurations, preparation and application in secondary metal (Li, Na, K, Mg, Al)-ion batteries. *Energy and Environmental Science* **12**: 2030 - 2053. DOI: <https://doi.org/10.1039/C8EE03014F>.
- Liang, J., Jiao, Y., Jaroniec, M. and Qiao, S.Z. (2012). Sulfur and nitrogen dual-doped mesoporous graphene electrocatalyst for oxygen reduction with synergistically enhanced performance. *Angewandte Chemie International Edition* **51**: 11496 - 11500. DOI: <https://doi.org/10.1002/ange.201208086>.
- Lu, J., Zhang, X., Zhang, X., Liu, N., Li, H., Yu, Z. and Yan, X. (2015). Electrochemical sensor for mercuric chloride based on graphene-MnO<sub>2</sub> composite as recognition element. *Electrochimica Acta* **174**: 221- 229. DOI: <https://doi.org/10.1016/j.electacta.2015.05.181>.
- MacDougall, D., Crummett, W.B., et al., (1980). Guidelines for data acquisition and data quality evaluation in environmental chemistry. *Analytical Chemistry* **52**: 2242 - 2249. DOI: <https://doi.org/10.1021/ac50064a004>.
- Marcolino-Junior, L.H., Janegitz, B.C., Lourenção, B.C. and Fatibello-Filho, O. (2007). Anodic stripping voltammetric determination of mercury in water using a chitosan-modified carbon paste electrode. *Analytical Letters* **40**: 3119 - 3128. DOI: <https://doi.org/10.1080/00032710701645463>.
- Martín-Yerga, D., González-García, M.B. and Costa-García, A. (2012). Use of nanohybrid materials as electrochemical transducers for mercury sensors. *Sensors and Actuators B: Chemical* **165**: 143 - 150. DOI: <https://doi.org/10.1016/j.snb.2012.02.031>.
- Martín-Yerga, D., González-García, M.B. and Costa-García, A. (2013). Electrochemical determination of mercury: a review. *Talanta* **116**: 1091-1104. DOI: <https://doi.org/10.1016/j.talanta.2013.07.056>.
- Martins, T.B., Miwa, R.H., da Silva, A.J.R. and Fazzio, A. (2007). Electronic and transport properties of boron-doped graphene nanoribbons. *Physical Review Letters* **98**: 196803. DOI: <https://doi.org/10.1103/PhysRevLett.98.196803>.
- Marton, D., Boyd, K.J., Al-Bayati, A.H., Todorov, S.S. and Rabalais, J.W. (1994). Carbon nitride deposited using energetic species: a two-phase system. *Physical Review Letters* **73**: 118-121. DOI: <https://doi.org/10.1103/PhysRevLett.73.118>.
- Nethravathi, C. and Rajamathi, M. (2008). Chemically modified graphene sheets produced by the solvothermal reduction of colloidal dispersions of graphite oxide. *Carbon* **46**: 1994 - 1998. DOI: <https://doi.org/10.1016/j.carbon.2008.08.013>.
- Ouyang, R., Zhu, Z., Tatum, C.E., Chambers, J.Q. and Xue, Z.L. (2011). Simultaneous stripping detection of Zn(II), Cd(II), and Pb(II) using a bimetallic Hg-Bi/single-walled carbon nanotubes composite electrode. *Journal of Electroanalytical Chemistry* **656**: 78 - 84. DOI: <https://doi.org/10.1016/j.jelechem.2011.01.006>.
- Pinilla, J.M., Hernández, L. and Conesa, A.J. (1996). Determination of mercury by open circuit adsorption stripping voltammetry on a platinum disk electrode.

- Analytica Chimica Acta* **319**: 25 - 30. DOI: [https://doi.org/10.1016/0003-2670\(95\)00469-6](https://doi.org/10.1016/0003-2670(95)00469-6).
- Rajabi, H.R., Roushani, M. and Shamsipur, M. (2013). Development of a highly selective voltammetric sensor for nanomolar detection of mercury ions using glassy carbon electrode modified with a novel ion imprinted polymeric nanobeads and multi-wall carbon nanotubes. *Journal of Electroanalytical Chemistry* **693**: 16-22. DOI: <https://doi.org/10.1016/j.jelechem.2013.01.003>.
- Ronning, C., Feldermann, H., Merk, R., Hofsäss, H., Reinke, P. and Thiele, J.U. (1998). Carbon nitride deposited using energetic species: a review on XPS studies. *Physical Review B* **58**: 2207-2215. DOI: <https://doi.org/10.1103/PhysRevB.58.2207>.
- Sahoo, P.K., Sahoo, S., Satpati, A.K. and Bahadur, D. (2015). Solvothermal synthesis of reduced graphene oxide/Au nanocomposite-modified electrode for the determination of inorganic mercury and electrochemical oxidation of toxic phenolic compounds. *Electrochimica Acta* **180**: 1023-1032. DOI: <https://doi.org/10.1016/j.electacta.2015.09.018>.
- Scidà, A., Haque, S., Treossi, E., Robinson, A., Smerzi, S., Ravesi, S., Borini, S. and Palermo, V. (2018). Application of graphene-based flexible antennas in consumer electronic devices. *Materials Today* **21**: 223-230. DOI: <https://doi.org/10.1016/j.mattod.2018.01.007>.
- Suenaga, K., Yudasaka, M., Colliex, C. and Iijima, S. (2000). Radially modulated nitrogen distribution in CN<sub>x</sub> nanotubular structures prepared by CVD using Ni phthalocyanine. *Chemical Physics Letters* **316**: 365 - 372. DOI: [https://doi.org/10.1016/S0009-2614\(99\)01340-8](https://doi.org/10.1016/S0009-2614(99)01340-8).
- Szörényi, T., Fuchs, C., Fogarassy, E., Hommet, J. and Le Normand, F. (2000). Chemical analysis of pulsed laser deposited a-CN<sub>x</sub> films by comparative infrared and X-ray photoelectron spectroscopies. *Surface and Coatings Technology* **125**: 308 - 312. DOI: [https://doi.org/10.1016/S0257-8972\(99\)00580-0](https://doi.org/10.1016/S0257-8972(99)00580-0).
- Velempini T. and Pillay K. (2019). Sulphur functionalized materials for Hg(II) adsorption: A review. *Journal of Environmental Chemical Engineering* **7**(5): 21. DOI: <https://doi.org/10.1016/j.jece.2019.103350>.
- Wanekaya, A.K. (2011). Applications of nanoscale carbon-based materials in heavy metal sensing and detection. *Analyst* **136**: 4383 - 4391. DOI: <https://doi.org/10.1039/c1an15574a>.
- Wang, Q., Kim, D., Dionysiou, D.D., Sorial, G.A. and Timberlake, D. (2004). Sources and remediation for mercury contamination in aquatic systems-a literature review. *Environmental Pollution* **131**: 323 - 336. DOI: <https://doi.org/10.1016/j.envpol.2004.01.010>.
- Wei, D., Liu, Y., Wang, Y., Zhang, H., Huang, L. and Yu, G. (2009). Synthesis of N-doped graphene by chemical vapor deposition and its electrical properties. *Nano Letters* **9**: 1752-1758. DOI: <https://doi.org/10.1021/nl803279t>.
- Wen, G.L., Zhao, W., Chen, X., Liu, J.Q., Wang, Y., Zhang, Y., Huang, Z.J. and Wu, Y.C. (2018). N-doped reduced graphene oxide /MnO<sub>2</sub> nanocomposite for electrochemical detection of Hg<sup>2+</sup> by square wave stripping voltammetry. *Electrochimica Acta* **291**: 95-102. DOI: <https://doi.org/10.1016/j.electacta.2018.08.121>.
- Wu, H.P. (1996). Dynamics and performance of fast linear scan anodic stripping voltammetry of cd, pb, and cu using in situ-generated ultrathin mercury films. *Analytical Chemistry* **68**: 1639 - 1645. DOI: <https://doi.org/10.1021/ac950879e>.
- Wu, Y., Fang, S. and Jiang, Y. (1999). Effects of nitrogen on the carbon anode of a lithium secondary battery. *Solid State Ionics* **120**: 117-123. DOI: [https://doi.org/10.1016/S0167-2738\(98\)00158-1](https://doi.org/10.1016/S0167-2738(98)00158-1).
- Xiong, S., Yang, B., Cai, D., Qiu, G. and Wu, Z. (2015). Individual and simultaneous stripping voltammetric and mutual interference analysis of Cd<sup>2+</sup>, Pb<sup>2+</sup>, and Hg<sup>2+</sup> with reduced graphene oxide-Fe<sub>3</sub>O<sub>4</sub> nanocomposites. *Electrochimica Acta* **185**: 52-61. DOI: <https://doi.org/10.1016/j.electacta.2015.10.114>.
- Xu, R.X., Yu, X.Y., Gao, C., Jiang, Y.J., Han, D.D., Liu, J.H. and Huang, X.J. (2013). Non-conductive nanomaterial enhanced electrochemical response in stripping voltammetry: The use of nanostructured magnesium silicate hollow spheres for heavy metal ions detection. *Analytica Chimica Acta* **790**: 31 - 38.
- Zhang, Y., Xie, J., Liu, Y., Pang, P., Feng, L., Wang, H., Wu, Z. and Yang, W. (2015). Simple and signal-off electrochemical biosensor for mercury(II) based on thymine-mercury-thymine hybridization directly on graphene. *Electrochimica Acta* **170**: 210-217. DOI: <https://doi.org/10.1016/j.electacta.2015.10.114>.
- Zhang, Z., Fu, X., Li, K., Liu, R., Peng, D., He, L., Wang, M., Zhang, H. and Zhou, L. (2016). One-step fabrication of electrochemical biosensor based on DNA-modified three-dimensional reduced graphene oxide and chitosan nanocomposite for highly sensitive detection of Hg(II). *Sensors and Actuators B: Chemical* **225**: 453-462. DOI: <https://doi.org/10.1016/j.electacta.2015.10.114>.
- Zhang, Z.J., Fan, S., Huang, J. and Lieber, C.M. (1996). Pulsed laser deposition and physical properties of carbon nitride thin films. *Journal of Electronic Materials* **25**: 57 - 61. DOI: <https://doi.org/10.1007/BF02666174>.
- Zhou, S.F., Han, X.J. and Liu, Y.Q. (2016). SWASV performance toward heavy metal ions based on a high-activity and simple magnetic chitosan sensing nanomaterials. *Journal of Alloys and Compounds* **684**: 1 - 7. DOI: <https://doi.org/10.1007/BF02666174>.
- Zhou, S.F., Wang, J.J., Gan, L., Han, X.J., Fan, H.L., Mei, L.Y., Huang, J. and Liu, Y.Q. (2017). Individual and simultaneous electrochemical detection toward heavy metal ions based on L-cysteine modified mesoporous MnFe<sub>2</sub>O<sub>4</sub> nanocrystal clusters. *Journal of Alloys and Compounds* **721**: 492-500. DOI: <https://doi.org/10.1007/BF02666174>.